Mechanics Research Communications 121 (2022) 103858

Contents lists available at ScienceDirect

Mechanics Research Communications

journal homepage: www.elsevier.com/locate/mechrescom

Controlled morphing of architected liquid crystal elastomer elements: modeling and simulations

Mattia P. Cosma, Roberto Brighenti *

Department of Engineering and Architecture, University of Parma, Parco Area delle Scienze 181/A, 43124 Parma, Italy

ARTICLE INFO

Keywords:
Liquid crystal elastomers
Stimuli-responsive materials
Architected materials
Morphing

ABSTRACT

Liquid crystal elastomers (LCE) are elastomeric materials possessing a network microstructure made of chains with a preferential orientation, induced by mesogen units embedded in the material prior to polymerization. This peculiarity can be harnessed to induce deformation of a LCE element by making its network to switch from the preferentially oriented nematic state to the isotropic one, as occurs for instance by rising the temperature above the transition value characteristic of the material. This mechanism can be combined with an architected arrangement of LCE blocks whose nematic orientation and transition temperature are properly differentiated among the different zones constituting the element. In this way, a controlled morphing can be obtained out of an architected elastomer made of LCE portions (ALCE), leading to a morphing structure whose deformation can be activated and precisely tuned by heating up or cooling down the material. In this research, we investigate architected LCE elements showing the capability of producing a variety of deformed shapes. A micromechanical theoretical model for LCE is firstly illustrated and several examples of morphing of architected LCE elements, whose mechanical response is obtained through finite element (FE) numerical analyses based on the proposed micromechanical model, are illustrated and critically discussed.

1. Introduction

To date, the possibility to produce materials showing particular intriguing properties, such as the controllable responsiveness to external stimuli or actions, has stimulated a huge research efforts, especially in the field of small-scale technological applications [1,2]. In this context, the capability of stimuli responsive materials of exhibiting large deformations leading to a noticeable shape change when properly stimulated (the so-called morphing), offers the potentiality to fabricate smart devices (nowadays also enabled by the available 3D printing technologies [3]), providing new attractive functionalities. These shape-change capabilities have been exploited, for instance, in soft robots where complex motions and shape-change (exploited to obtain bending, twisting and extension) are provided by the material structure itself, leading to a system with an unlimited number of degree of freedoms, without the need of an external tethered control as typically occurs for standard robots [4].

Several examples of controlled structural shape morphing, i.e. of structures that change shape in a controlled manner, can be found in the literature; for instance, some modular self-reconfigurable robots can morph from a snake-like structure into a quadruped walker or vice versa, thus allowing the robot to move through a narrow space to accomplish its tasks [5]. In nature, the complex motion of soft muscular structures can be achieved by a synergic actuation of many simple contractile elements , spatially and functionally properly arranged [6]. The morphing capability has also been obtained by harnessing the tensegrity concept through a modular design, coupling elastomeric cables, made of memory polymers, with strut elements, [7]. Morphing has also been obtained by exploiting differential surface wetting in soft structures or by assembling materials with different fluid diffusion length scales [8]. Residual stresses induced by some polymerization processes, such as the so-called photopolymerization, have shown the capability to provide structures with shape morphing characteristics, enabled by the shrinkage and distortion induced by a non-uniform laser exposure during the production process [9]. Finally, it is worth mentioning that morphing capabilities have also been obtained within the field of origami and kirigami functional materials [10,11].

Among the materials and structures enabling shape morphing, liquid crystal elastomers (LCEs) represent a charming class of responsive polymers that combine mechanical properties of both fluids and solids

* Corresponding author at: Univ. of Parma, Viale delle Scienze 181A, 43124 Parma, Italy.
E-mail address: brigh@unipr.it (R. Brighenti).

https://doi.org/10.1016/j.mechrescom.2022.103858
Received 22 December 2020; Received in revised form 7 September 2021; Accepted 9 February 2022
Available online 14 February 2022

[12–18]. In this context, experimental researches have shown the possibility to obtain shape programmable actuators through 3D printed structures with a controlled molecular order [19–21].

LCE materials exhibit large and reversible deformations when properly stimulated by environmental inputs; if we zoom into their microstructure, a spontaneous order of the chain network inferred by the molecular structure of liquid crystals (LCs) can be observed in some conditions (nematic state), while in other conditions they exhibit a disordered configuration, typical of standard polymeric matrices (isotropic state). Being the ordered-disordered transition phenomenon (nematic to isotropic) accompanied by large and reversibile deformations of the network, this class of material has been recognized to be particularly attractive for actuation and morphing [22]. As a matter of fact, the ordered-disordered transition of LCEs is usually triggered by heat or light (Fig. 1), leading to – when LCE mesostructure is properly architected – a responsive morphing material or device suitable for actuation.

The so-called nematic order is usually quantified through the order tensor describing the alignment of the mesogen units at the microscopic scale [15].

Depending on the type of LCE in turn, the variation of the nematic order can be induced by different triggering stimuli, ranging from heat, UV-light, electric or magnetic field [23–25].

For instance, the irradiation of the material with UV-light (photo-actuation mechanism), modifies the chain network arrangement (order-disruption) when the LCE material contains molecular units undergoing isomerization (such as the trans-cis chemical transformation taking place in azobenzene-based LCEs). On the other hand, the nematic-isotropic switching can be obtained by directly heating the material in which temperature-sensible mesogens have been embedded [26] (thermal actuation), or, indirectly, by light irradiation of LCEs doped with photo-thermal agents (such as gold nanoparticles, carbon nanotubes, graphene, etc.), leading to the photo-thermal actuation [27–30].

By harnessing the deformation capabilities of LCEs and by taking inspiration from the so-called metamaterials – whose properties come from the arrangement of their building blocks rather than from their mechanical properties [31,32] – we investigate the tunability of the responsiveness of a class of metamaterials, obtained by properly arranging LCE blocks, capable of showing a wide variety of controllable shape morphing induced by a temperature change. In the following, we refer to the above-mentioned elements as architected liquid crystal elastomers (ALCEs). By analogy with deformations occurring in nature for locomotion or peristaltic motion, we demonstrate the possibility to realize structural elements whose deformed shapes resemble that observed in several natural phenomena, which can be precisely controlled by changing the relevant environmental stimulus.

For this purpose, we introduce a theoretical model that, through a statistical-based description of the network chains arrangement, leads to a micromechanical model suitable to describe the mechanical response of polymers possessing a nematic order pattern characterized by different transition temperatures.

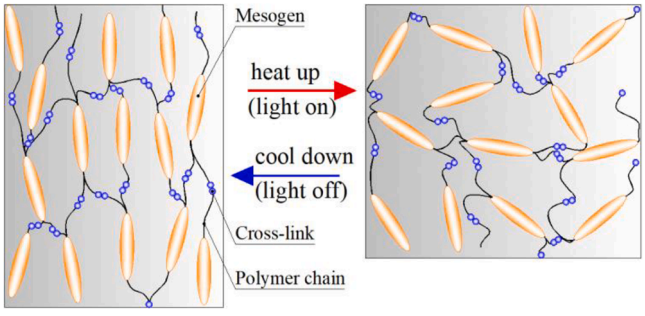

Fig. 1. Scheme of the ordered-disordered transition (i.e. from the nematic to the isotropic state) in a LCE element.

In the literature, various models have been proposed to predict the shape produced by changing the mesogens alignment in LCEs, allowing the inverse problem of designing the alignment patterns for prescribed morphing shapes to be obtained. Theoretical models based on the relationship between the orientation of the mesogen units in thin sheets or in simple bilayers and the corresponding arising curvature have been developed [33,34].

A stretch–temperature relation has been implemented into a FE (finite element) approach to model the shape morphing of LCEs; this approach has been used in [36] where experimental tests related to the photothermal light-induced shape-morphing of LCEs with a proper spatial pattern of gold nanoparticles concentration has been simulated.

In the present approach, we follow a different route: the variation of the statistical distribution of the polymer chains driven by the mesogens arrangement change (depending on the local temperature of the LCEs and, if it is the case, on the mechanical stress applied), is used to determine the local stress and deformation states of the material. No structural models have been introduced (such as the assumption typically made for thin plates, membrane or bilayer structural elements); from this viewpoint the proposed approach is suitable to model any arrangement of LCEs patterns with different mesogen orientation and/or transition temperature. The parameters involved in the model have a clear physical meaning and they can be easily related to the synthesis process of the material; the proposed approach is thus suitable to assess the obtainable shape morphing before fabricating the architected LCE element.

The proposed micromechanical model is then upscaled at the continuum level and implemented within a FE framework for the simulation of real case elements.

Various arrangements of LCE blocks – characterized by different nematic orders and, eventually, by different transition temperatures – are considered. Their shape morphing capabilities are quantitatively simulated through numerical analyses. It is shown how, by properly tuning some properties of the material at the mesoscale level (such as the arrangement of the constituent blocks of ALCEs or, more intriguingly, their transition temperature), a controlled shape-morphing can be achieved. Although the inverse problem of designing a specific pattern of mesogens suitable to obtain a prescribed shape-morphing is not a goal of the present work, the developed model is exploited for quantitatively illustrating how vast can be the obtainable responsiveness of a simple structural beam-like element.

From this perspective, this study provides an insight into the limitless possibilities to obtain the desired conformation from properly designed architected LCEs.

The paper is organized as follows: Sect. 2 deals with the mechanics of stimulus-responsive LCEs. Sect. 3 discusses the basic idea of ALCEs presenting a brief parallelism with bio-inspired structures. Numerical simulations devoted to predict the responsiveness of ALCEs are presented in Sect. 4 and, finally, Sect. 5 outlines some conclusions and future perspectives.

2. Mechanical behavior of stimulus-responsive LCE

2.1. Statistical based description of a polymer network

Standard polymer network consists of an amorphous arrangement of entangled linear chains – each one assumed to be made of N rigid (Khun's) segments of equal length b, arranged in space according to the random-walk theory – whose physical state, according to the Freely-Join-Chain (FJC) assumption, depends only on the so called end-to-end vector $\boldsymbol{r}$ [15,37]. The chains are linked together at discrete points, termed as cross-links, forming the network. The chains arrangement in the 3D space, quantified by the statistical distribution $\rho_0(\boldsymbol{r})$ of the end-to-end vectors $\boldsymbol{r}$, allows us to determine the mechanical state of the polymer [37]. In the stress-free state, the distribution of the end-to-end vectors is usually assumed to follow the standard 3D Gaussian

distribution, i.e. $\rho_0(\boldsymbol{r}) = c_a\varphi_0(\boldsymbol{r})$, being c_a the number of mechanically active chains (i.e. chains joined to the network at both extremities), and φ_0 the normalized Gaussian distribution function, $\varphi_0(|\boldsymbol{r}|) = \left(\frac{3}{2\pi Nb^2}\right)^{\frac{3}{2}}\exp\left(-\frac{3|\boldsymbol{r}|^2}{2Nb^2}\right)$.

The knowledge of the chain distribution change, from the stress-free state to the actual one (accounting for the mechanical deformation of the network, and eventually for chains breakage, time-related effects as well as the ordered-disordered network transition occurring in LCEs), provides all the information required to describe the mechanical state of the polymer in the current state [38].

In polymer physics, the mechanical energy stored in a single chain is usually assumed to depend on the end-to-end vector length $|\boldsymbol{r}|$. According to the Gaussian statistics [39] valid for moderate chain stretch values, the elastic energy of a single chain is expressed as $\psi(\boldsymbol{r}) = \frac{3k_BT}{2Nb^2}|\boldsymbol{r}|^2$ The potential elastic energy per unit volume of the polymer, evaluated with respect to the stress-free state, is given by:

$$\Delta\Psi = \Psi - \Psi_0 = \int_{\Omega}[\rho(\boldsymbol{r},t) - \rho_0(\boldsymbol{r})]\psi\, d\Omega \tag{1}$$

Alternatively, Eq. (1) can be rewritten as follows [40]:

$$\Delta\Psi = \frac{3c_ak_BT}{2Nb^2}\mathrm{tr}(\boldsymbol{\mu} - \boldsymbol{\mu}_0) + p[\det \boldsymbol{F} - 1] \tag{2}$$

where p is the hydrostatic pressure required to enforce the incompressibility constraint (expressed by $\det \boldsymbol{F} = 1$, being $\boldsymbol{F}$ the deformation gradient tensor) here assumed. In Eq. (2), the distribution tensors providing the covariance matrices of the distribution of $\boldsymbol{r}$ in the current and in the initial stress-free state, $\boldsymbol{\mu} = \langle\varphi\boldsymbol{r}\otimes\boldsymbol{r}\rangle$and$\boldsymbol{\mu}_0 = \langle\varphi_0\boldsymbol{r}\otimes\boldsymbol{r}\rangle$, have been introduced, while $\langle\blacksquare\rangle$ indicates the integration of $\blacksquare$ over the chain configuration space Ω [38]. If the affine deformation hypothesis holds true, the chain stretch vector is given by $\boldsymbol{\lambda} = \boldsymbol{r}/|\boldsymbol{r}_0|$ and the distribution tensor in the current state becomes $\boldsymbol{\mu} = \langle\varphi\boldsymbol{\lambda}\otimes\boldsymbol{\lambda}\rangle|\boldsymbol{r}_0|^2$. Such a tensor contains the information related to the average chain stretch in different directions; in its principal directions frame of reference identified by the versors $\boldsymbol{m}_i$, it is written as $\boldsymbol{\mu}_d = \mu_i\boldsymbol{m}_i\otimes\boldsymbol{m}_i(i = 1, 2, 3)$ where μ_i are the eigenvalues of $\boldsymbol{\mu}$ and the Einstein summation convention has been used (in the following, the subscript d *is* omitted for sake of simplicity). The distribution tensor $\boldsymbol{\mu}$ provides the information related to the spatial distribution of the network chains and so every action influencing such a distribution reflects on $\boldsymbol{\mu}$ whose knowledge suffices to determine the mechanical state of the polymer.

2.2. Thermally-driven chains rearrangement: from standard polymer network to LCE

When a LCE polymer network in the nematic state is considered, its mesogens units are preferentially oriented in one direction and the normalized Gaussian function of the polymer chains distribution φ_0 is non-isotropic [40]. The so-called order parameter quantifying the average global degree of the mesogens alignment, is defined as $Q = <\frac{3}{2}\cos^2\theta - \frac{1}{2}>$ [15] (where θ is the angle formed by the mesogen local axes $\boldsymbol{u}$ and the nematic director $\boldsymbol{n}$, the latter pointing along the average direction of alignment). By assuming the mesogens to be preferentially oriented along the $x-$ direction of the Cartesian frame of reference, i.e. $\boldsymbol{n}\equiv\boldsymbol{x}$, the distribution tensor becomes:

$$\boldsymbol{\mu}_n = \frac{Nb^2}{3}\begin{bmatrix} 1+2Q & 0 & 0 \\ 0 & 1-Q & 0 \\ 0 & 0 & 1-Q \end{bmatrix} \tag{3}$$

In the case the mesogen units are perfectly aligned along the $x-$ axis, then $Q = 1$ (θ is either equal to 0 or π), while the value $Q = 0$ indicates randomly oriented rods as occurs in a perfectly isotropic arrangement of chains for which $\langle\cos^2\theta\rangle = 1/3$ and $\boldsymbol{\mu}_n = \frac{Nb^2}{3}\,\mathbf{1}$. Values of Q falling in the range $0\div1$ indicate a non-perfect alignment, with an increasing degree of dispersion along the nematic director as $Q\to 0$. Finally, when $Q = -1/2$, all the LC rods belong to the $y-z$ plane. If the director varies in space, it is convenient to introduce the order tensor $\boldsymbol{Q} = Q_{ij} = \frac{Q(T)}{2}(3n_in_j - \delta_{ij})$ where $\boldsymbol{n}$=n_i is the above-introduced global nematic director [15,13]. It is worth mentioning that the order tensor is related to the distribution tensor as shown in [40].

Finally, the stress state of the material is provided by [40,41]:

$$\boldsymbol{\sigma} = J^{-1}\boldsymbol{P}\boldsymbol{F}^T = \frac{3c_ak_BT}{Nb^2}(\boldsymbol{\mu} - \boldsymbol{\mu}_{0n}) + p\boldsymbol{I},\ \ with\ \boldsymbol{P} = \frac{\partial\Delta\Psi}{\partial\boldsymbol{F}} \tag{4}$$

where $\boldsymbol{\sigma}, \boldsymbol{PP}$ are the Cauchy and the first Piola stress tensors, respectively. It is worth mentioning that, when a LCE network is considered, the distribution tensor which appears in the definition of the stress state of the material (Eq. (4)), must be assessed accordingly. In this case, the initial distribution tensor of the nematic LCE network, assumed herein to coincide with the stress-free state of the material, is $\boldsymbol{\mu}_{0n} = \boldsymbol{\mu}(t=0) = \boldsymbol{\mu}_n(Q = Q_0)$, see Eq. (3). The current distribution tensor $\boldsymbol{\mu}(t)$ is affected by both the order change induced by the temperature variation as well as by the applied mechanical deformation; thus, its time rate $\dot{\boldsymbol{\mu}}(t)$ can be expressed by adding up these two above-mentioned contributions:

$$\dot{\boldsymbol{\mu}}(t) = \dot{\boldsymbol{\mu}}_m(t) + \dot{\boldsymbol{\mu}}_n(t) \tag{5}$$

where $\dot{\boldsymbol{\mu}}_m$ represents the effect of the mechanical stress while $\dot{\boldsymbol{\mu}}_n$ is the rate associated with the temperature-dependent change of the nematic order. The above rates are given by [40]:

$$\dot{\boldsymbol{\mu}}_m = \left.\frac{\partial\boldsymbol{\mu}(t)}{\partial t}\right|_n =< \varphi(t)\,\boldsymbol{r}\otimes\boldsymbol{r} > \boldsymbol{L}(t) = \boldsymbol{L}(t)\boldsymbol{\mu}(t) + [\boldsymbol{L}(t)\boldsymbol{\mu}(t)]^T \tag{6a}$$

$$\dot{\boldsymbol{\mu}}_n(t) = \left.\frac{\partial\boldsymbol{\mu}(t)}{\partial t}\right|_m = 2\frac{Nb^2}{3}[\dot{\boldsymbol{Q}}(t) - \boldsymbol{W}(t)\boldsymbol{Q}(t) + \boldsymbol{Q}(t)\boldsymbol{W}(t)] \tag{6b}$$

where $\blacksquare|_n$, $\blacksquare|_m$ indicate the quantity $\blacksquare$ evaluated at constant nematic order parameter and at constant applied mechanical deformation, respectively, while $\boldsymbol{W} = 1/2(\nabla\dot{\boldsymbol{u}} - \nabla\dot{\boldsymbol{u}}^T)$ is the spin tensor. The distribution tensor $\boldsymbol{\mu}$ at the generic time t can be obtained by integrating the above rates in the time domain $(0, t)$ as $\boldsymbol{\mu}(t) = \boldsymbol{\mu}(0) + \int_0^t[\dot{\boldsymbol{\mu}}_m(\tau) + \dot{\boldsymbol{\mu}}_n(\tau)]d\tau$.

In the case the order parameter depends on the temperature while the principal directions of $\boldsymbol{Q}$ do not change, $\dot{\boldsymbol{Q}}(t)$ in Eq. (6b) is given by

$$\dot{\boldsymbol{Q}}(t) = \frac{1}{2}\frac{\dot{\ell}(t)}{b}$$
$$\text{with } \dot{\ell}(t) = b\dot{Q}(t)\ [3\,\boldsymbol{n}\otimes\boldsymbol{n} - 1],\ \dot{Q}(t) = \frac{\partial Q(T)}{\partial T}\dot{T} \tag{7}$$

being ℓ the so-called step length tensor.

The nematic order of the LCE can be related to the temperature of the material in a way that $Q = Q_0$ when $T < T_{NI}$, while $Q\to 0$ if $T > T_{NI}$, where T and T_{NI} are the current and the nematic-isotropic transition temperature, respectively, while Q_0 is the initial value of the order parameter of the LCE network.

The $Q - T$ relationship used for determining the nematic-isotropic evolution counterpart of the distribution tensor (see Eq. (6b), depends on the chemical-physics properties of the material and can be determined from experimental tests [43]; it quantifies the transition of the order parameter from its initial value Q_0 to the current one at the temperature T. Here, we adopt an expression for $Q - T$ in the form $Q(T) = Q_0f(T)$, with $f(T) = \left[1 + \exp\frac{T-T_{NI}}{c}\right]^{-1}$, being c a material-dependent parameter.

The $Q - T$ curves plotted by assuming different values of the

parameter c are shown in Fig. 2(c); the comparison with the experimentally obtained order parameter measured on a monodomain nematic elastomer (y – oriented) shows a reasonable similar trend. Starting from a known nematic configuration with $Q_0 = 0.46$at $T = 20°C$, we heat up the material up to a temperature above the nematic-transition temperature $T_{NI} = 86°C$[42] in order to recover the isotropic state. The material-dependent parameter c influences the nematic-isotropic transition, leading to sharp change (lower values of c) or more gradual ones (higher values of c), Fig. 2(c). The deformed shapes of the strip resulting from FE analysis for two values of c at a given temperature $T^* = 70°C$, are reported in Fig. 2(d): the contraction along the nematic direction is lower for lower c ($\lambda_y = 0.98$, A) since Q remains practically unchanged until the temperature value T^* is reached ($c = 5$, point A, Fig. 2(c)); on the other hand, at the same temperature, Q is lower for a higher c (point B, Fig. 2(c)) corresponding to a more evident contraction ($\lambda_y = 0.88$, B, Fig. 2(d)).

3. From bio-inspired morphing to architected liquid crystal elastomers

3.1. Bio-inspired materials architectures

The fascinating architectures of natural structures (ranging from wood, antler, bone and teeth, silk, fish scales, bird beaks, insect wings, shells, etc.) are increasingly attracting the interest of researchers because of their mechanical functionality and effectiveness. In fact, the above-mentioned structures have usually an optimum weight to strength ratio, allowing to safely bear mechanical stress by using the least amount of material. Soft-bodied animals (such as octopus, caterpillars, snakes, maggots, etc.) are able to deform in a complex way with the aim to show a desired functionality; for instance, among the most useful functionalities in nature, locomotion represents a crucial task to be efficiently done for survival purpose. Shape-morphing strategy represents an efficient way for small organism to move in a viscous fluid where the kinematic-reversible mechanism, typically used at high Reynolds numbers, doesn't work. Soft natural living matter is thus a source of inspiration for the development of engineered artificial materials and devices mimicking functionalities observable in nature [44–47].

Natural structures display intricate architectures – ranging from the nano-, micro- and meso-scale size – reflecting an impressive range of different functionalities; arrangement, orientations and features of individual structural units are often optimized to get the best overall behavior, to perform in the best way specific biological functions or to protect themselves by the surrounding, i.e. to ensure the optimum maximization of survival and longevity [48]. Natural structures properly respond to certain environmental conditions or to peculiar external stimuli: examples are represented by "pill bugs" (*armadillidium vulgare*, terrestrial isopods), capable of morphing for protecting themselves against predators by means of conglobation morphing, the ability to roll up into a ball when stimulated by strong vibrations or pressure exerted by predators.

It is worth mentioning that morphing in nature can also take place in a more general way; social animals (such as fire ants, honey bees, etc.) can aggregate in swarms made of many individuals joined together [49]; this strategy allows forming a super-organism (or cluster) whose shape changes according to different stimuli in order to fulfill some goal such as mechanical stability or thermal comfort [50,51]. Opposite to the above-cited collective behavior, single cell organisms (such as individual cells) morph to produce motility [52]. Inspired by morphing of highly deformable organisms, the development of continuum materials whose architecture is made of blocks with a controllable deformation, paves the way to create simple and efficient soft actuators with unlimited morphing capabilities.

3.2. LCE-based metamaterials

When properly stimulated, the deformation potentialities of LCEs offer the opportunity to create architected elements by a suitable assembling of LCE portions having different nematic directors and/or transition temperatures; this allows the production of soft actuators whose morphing capability can be precisely tuned (controlled morphing) [26,53]. The production of architected LCE-based elements is

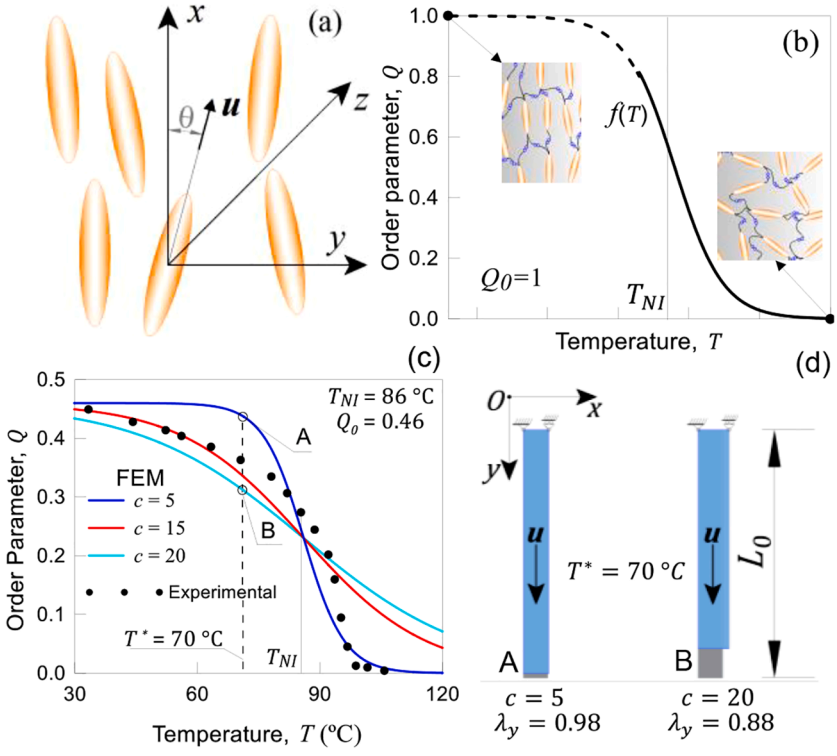

Fig. 2. (a) Scheme of the preferential orientation of liquid crystal molecules with local axes $\boldsymbol{u}$ fluctuating around the nematic director $\boldsymbol{n}\equiv\boldsymbol{x}$. (b) Ordered-disordered transition in LCE due to a temperature increase (from left to right). (c) $Q - T$ curves obtained through the function $f(T)$ for different values of the material-dependent parameter c, compared with experimental values [42]. (d) Deformed shapes of the considered element at a given T for two values of the parameter c (obtained from FE simulations).

nowadays possible and affordable thanks to the modern additive manufacturing production technologies [20,21,23,35,54,55]. The easiest way to get a LCE-based metamaterial consists in arranging LCE regions characterized by distinct nematic directors into a bilayer structure; upon a thermal stimulus, this induces a bending-like deformation through the thickness due to expansion/contraction mismatch, allowing to get, if required, elements characterized by wavy-like deformed shapes. A first experimental attempt to mimic the wavy-like morphing of an element can be found in [56], where two LCE layers joined together have been used to induce bending morphing.

In other words, a bi-layer of LCE material can form a localized hinge which provides a localized rotation induced by alternate tensile/compressive strain along the element thickness; controlling the position and the geometric-related features (geometrical size, nematic director orientation, etc.) of these LCE hinges, coupled with inert parts of material (blue blocks of Fig. 3), can be exploited to obtain elements with intriguing tunable shape-morphing capabilities (Fig. 3).

Being LCE-based actuators capable of developing an actuation power of the order of $10^5 \mathrm{J/m}^3$ [57], they can be employed in a variety of applications, such as in soft robots, tunable stereoscopic displays, intelligent skin, grippers, etc.

4. Numerical simulations

4.1. Numerical implementation

The micromechanical model illustrated above can be readily implemented into a FE computational framework. To this end, it is convenient to introduce the variational statement of the problem that reads:

$$\begin{aligned}\delta_{\boldsymbol{u}}\Pi = \delta_{\boldsymbol{u}}\Psi_e + \delta_{\boldsymbol{u}}\Psi_{ext} &= \int_{\mathscr{B}_0} \frac{\partial \Psi}{\partial \nabla \boldsymbol{u}} \delta \nabla \boldsymbol{u}\, dV - \int_{\mathscr{B}_0} \boldsymbol{B}\cdot\delta\boldsymbol{u}\, dV - \int_{\partial\mathscr{B}_0} \boldsymbol{t}\cdot\delta\boldsymbol{u}\, dA \\ &= \int_{\mathscr{B}_0} [\nabla\cdot\boldsymbol{P} - \boldsymbol{B}]\delta\boldsymbol{u} dV + \int_{\partial\mathscr{B}_0} [\boldsymbol{P}\cdot\boldsymbol{N} - \boldsymbol{t}]\cdot\delta\boldsymbol{u} dA = 0\end{aligned} \tag{8}$$

being $\boldsymbol{P} = \boldsymbol{J}\boldsymbol{\sigma}\boldsymbol{F}^{-T} = \partial\boldsymbol{\Psi}/\partial\nabla\boldsymbol{u}$ the first Piola stress tensor, while $\boldsymbol{B}$, $\boldsymbol{t}$ are the body and traction forces in the reference configuration and $\boldsymbol{N}$ is the unit outward normal to the boundary. By introducing the FE discretization of the displacement field and of its gradient,

$$\boldsymbol{u}_a = \sum_{i=1}^{n_n} [N]_i \widetilde{\boldsymbol{u}}_i,\ \ \nabla\cdot\boldsymbol{u}_p = \nabla_X \sum_{i=1}^{n_n} [N]_i \widetilde{\boldsymbol{u}}_i = \sum_{i=1}^{n_n} [B]_i \widetilde{\boldsymbol{u}}_i. \tag{9}$$

(being $\blacksquare_a$ and $\widetilde{\blacksquare}$ the interpolated and the nodal values of the quantity $\blacksquare$)

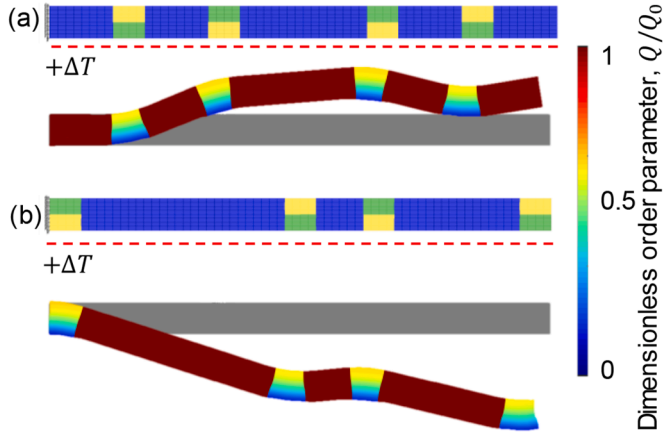

Fig. 3. Examples of generic deformed shapes predicetd by the present model, obtainable by thermal-triggered morphing of an element made of properly arranged LCE parts with different nematic directors, coupled with inert parts of material.

the variational statement (Eq. (8)) leads to the following equilibrium equation written in terms of the unbalanced residual nodal force vector

$$\{R\}_{\boldsymbol{u}}^e = \int_{V_0^e} [B]^T \boldsymbol{P}\, dV - \int_{V_0^e} [N]^T \boldsymbol{B} dV + \int_{A_0^e} [N]^T \boldsymbol{t} dA = \{0\} \tag{10}$$

where the single finite element e with volume V_0^e and boundary surface A_0^e has been considered. It can be noticed that the knowledge of the stress field at the FE Gauss points allows evaluating the vector of the unbalanced residual forces whose norm must fulfill some convergence requirements through an iterative procedure, for example by using the standard Newton method [40].

4.2. Numerical simulations and discussion

This section is devoted to illustrate the controlled morphing of architected LCE-based elements through numerical simulations; the examined cases, consisting in a simple rectangular 2D beam-like element made of LCEs units – alternatively arranged by changing their nematic directors and the characteristic transition temperature – outline the huge variety of shape morphing obtainable from an architected LCE cantilever beam. Elements made of LCE blocks arranged as shown in Fig. 4 , each one characterized by distinct widths of the constituent LCE blocks, namely $w/L = 0.125$; 0.25; 0.5 (Fig. 4, top-to-bottom elements) are considered. The height of each LCE block is assumed to be one half of the height of the beam-like element and is kept fixed for the three investigated patterns. As can be appreciated from the detail of Fig. 4, the element is assumed to be made of LCE blocks having different nematic orientations, namely LC_Y blocks (green regions in Fig. 4) and the LC_X blocks (yellow regions in Fig. 4), corresponding to mesogen units with nematic director along the y-axis and x-axis, respectively. We investigate the role played by different relative sizes of LCE rectangular blocks within the element, whose nematic mesogens orientations and/or nematic-isotropic transition temperatures T_{NI} differ from block to block, in triggering different shape morphing for different boundary constraints.

In the first example, we consider an element made of a pattern of appropriately assembled LCE blocks having the same T_{NI}. Then, we illustrate the controlled morphing of an element made of a fixed pattern of LCE blocks but with different T_{NI}.

Hereafter, we consider a rectangular beam-like element whose geometry in the undeformed state is characterized by $L/h = 16$, $h = 500\mu m$ and thickness $t = h$. Moreover, we adopt a constant shear modulus of the material $\mu = 13.33kPa$ that, for sake of simplicity, is assumed to be temperature-independent. The analyses are performed by assuming a

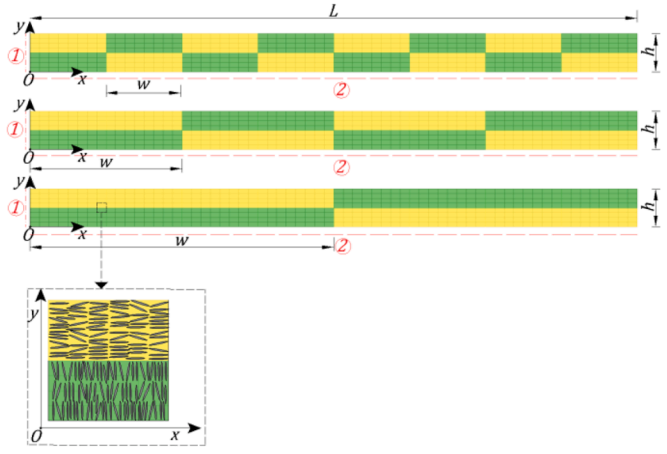

Fig. 4. Arrangement of LCE blocks with two nematic order orientations, yellow along x, green along y, organized in architected patterns; three different dimensionless ratios w/L are adopted.

plane stress condition and a fast heating because of the small size of the element. In the examples, the temperature of the bottom surface of the element is increased from $T_B = 25°C$ to $T_B = 150°C$. The temperature evolution within the material is determined by solving the heat conduction problem in the element's domain whose thermal conductivity and specific heat are assumed to be $\kappa = 0.2$ W/mK and $C = 1050$ J/Kg K, respectively. In order to not have further deformations not related to the nematic-isotropic transition of the LCE parts, the thermal expansion of the material is neglected within the temperature range considered.

Unless differently stated, we assume the nematic-isotropic transition temperature to occur at $T_{NI} = 50°C$, while the parameters describing the transition from the initial nematic to the final isotropic state are assumed to be $Q_0 = 0.3$ and $c = 20$ for all the LCE blocks.

We implemented the micromechanical model outlined above into a FE framework for simulating the morphing behavior; firstly, we investigate the morphing response of ALCE elements, assumed to be fabricated according to the three patterns shown in Fig. 4. The deformation response is studied by adopting either a clamped boundary condition (BC) along the edge ① (displacements $\delta_x = \delta_y = 0$ at $X = 0$) or a simply supported element along the edge ②, i.e. lying on a rigid horizontal frictionless plane (unilateral constraint, displacements $\delta_y \geq 0$ at $Y = 0$), see Fig. 4.

The results related to the cantilever elements are reported in Fig. 5; the deformed shapes of the centreline for three different temperature levels ($T_B/T_{NI} = 0.7$; 1.0; 1.5) and the corresponding deformed shapes of the element for $T_B/T_{NI} = 1$ for the three patterns of Fig. 4 ($w/L = 0.125$, 0.25, 0.5), are illustrated. As it can be noticed, the coupling of LCE blocks in a proper architected way provides alternate zone of compressive/tensile strain within the element, resulting in a wavy-like shape morphing. Further, it can be appreciated that the right-hand side of the element move upwards upon rising the temperature: at a fixed T_B/T_{NI} value, the higher the w/L, the higher the uplift displacement obtained.

We consider now the results related to the architected LCE element lying on a rigid frictionless plane; Fig. 6 illustrates the LCE-temperature-dependent deformation of the centreline of the considered element. Similarly to the previous case, the architected LCE element is characterized by wavy-like deformed shapes whose amplitudes depend on the ratio w/L.

In this case, due to the different BCs with respect to those of the cantilever element, the amplitude of the deformed shapes are less pronounced at a fixed values of w/L and T_B/T_{NI}.

In the last example, we consider the morphing of a cantilever element whose LCE blocks have both different nematic orientation and transition temperatures; $T_{NI,X} = 50°C$ has been assumed for zones with mesogens preferentially oriented along X, while $T_{NI,Y}$ is equal to either 50, 70, 100, $130°C$ for zones with mesogens preferentially oriented along Y (cases no. 1, 2, 3, 4, respectively, in Fig. 7a,b). This leads to a controlled morphing of the element due to an asynchronized thermo-mechanical responsiveness, allowing, for example, to make the material point P_0 capable of following a desired displacement path during the temperature increase (see Fig. 7a). Let's image to require the point P_0 to move from its initial position ($X = L$, $Y = 0$) to an assumed target zone (light-blue circle in Fig. 7a) following different trajectories. The use of LCE blocks with different activation temperatures $T_{NI,Y}$ allows the point to move from P_0 to the target area moving initially upward to the left (black paths, $T_{NI,Y} = 50$, $70°C$) or firstly downward and then upward to the left (red paths, $T_{NI,Y} = 100$, $130°C$), making the point capable, for example, to move toward the desired region by avoiding obstacles.

5. Conclusions and future developments

We have investigated the possibility to precisely control the shape

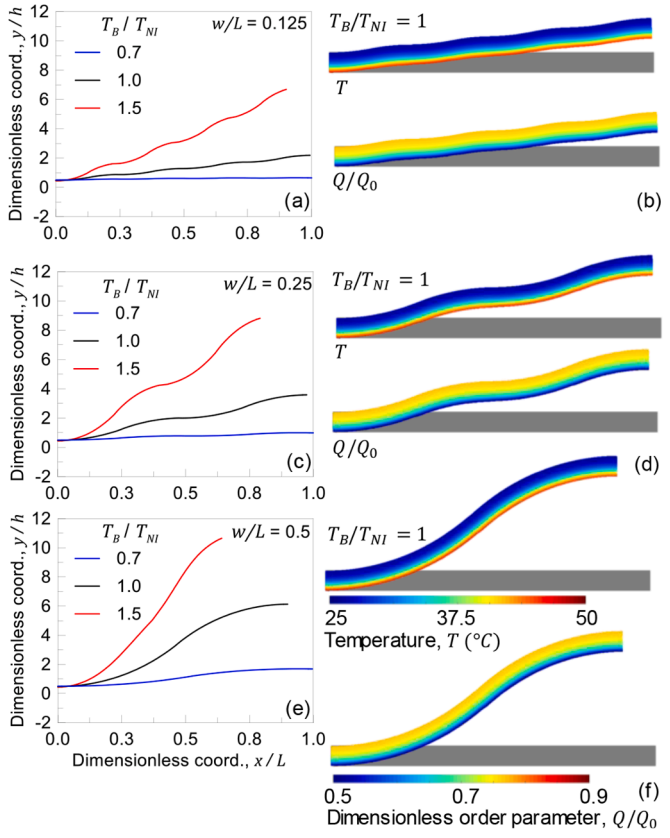

Fig. 5. Architected LCE cantilever element under a temperature increase (see Fig. 4). (a,c,e) centerline deformed shapes, and (b,d,f)corresponding deformed shapes with temperature and nematic order fields at $T_B/T_{NI} = 1$.

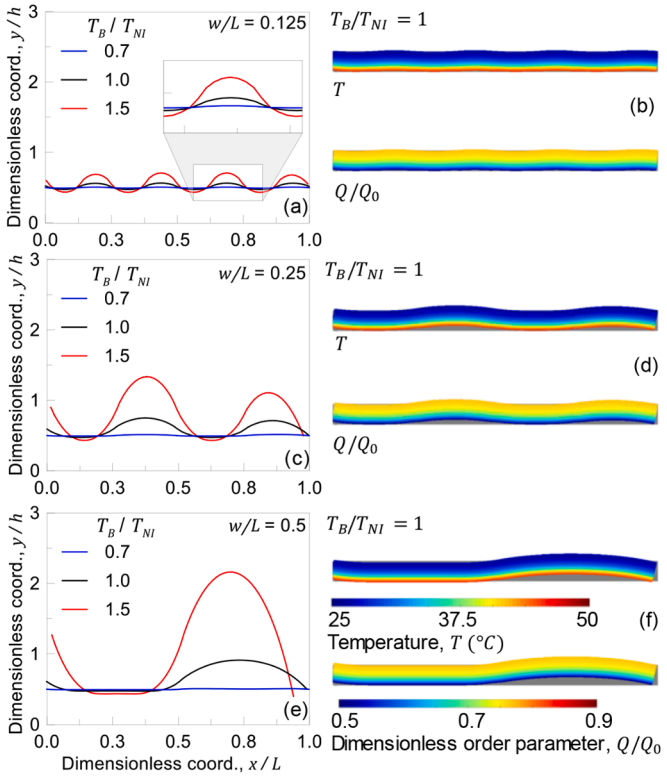

Fig. 6. Architected LCE element lying on a horizontal frictionless plane (see Fig. 4) stimulated by a temperature increase. (a,c,e) Centerline deformed shapes, and (b,d,f) corresponding deformed shapes with temperature and nematic order fields at $T_B/T_{NI} = 1$.

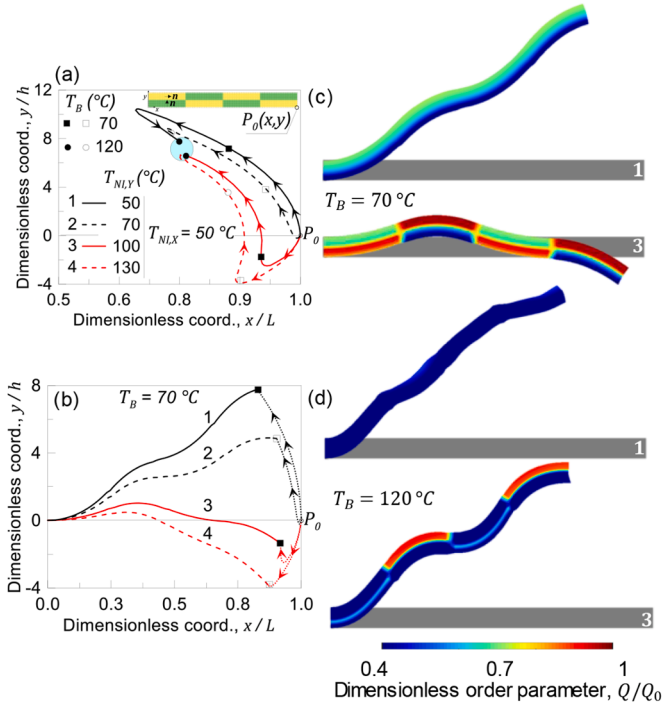

Fig. 7. Architected LCE cantilever element under a temperature increase. (a) paths of the point P obtained by rising the temperature T_B from 20°C to 120°C, (b) centerline deformed patterns and (c,d) corresponding element's deformed shapes with dimensionless nematic order maps.

morphing of elements made of architected blocks of LCE, aimed at obtaining desired functionalities. It has been considered a temperature-responsive LCE material whose transition from the nematic state to the isotropic one occurs when the transition temperature is overcome.

A general theoretical micromechanical-based framework, without any particular assumptions coming from the structural element considered, has been briefly illustrated and some numerical FE simulations, based on the FE implementation of the proposed theory, have been performed. It has been demonstrated that a proper arrangement of the LCE blocks with different nematic directors and/or transition temperatures, allows us to control the obtained deformed shapes, leading to a desired morphing whose deformation mechanism is capable to follow a preferential path. The present investigation, which considered a simple beam-like element, allows us to easily capture and predict quantitatively the role played by the LCE blocks arrangement (geometrical size, nematic directors orientation, transition temperature) on the controlled morphing. The results have demonstrated that a proper design of LCE-based elements represents a promising way to obtain fully tunable flexible systems displaying large reversible deformations with path-controllable displacements. The obtained results represent a starting point for the design and simulation of more complex engineering systems and devices. Within this context, a future important advancement will be the design of proper LCE pattern arrangements capable of producing a desired deformed shape under a given temperature history. This issue (suitable to be tackled by using, for example, Artificial Intelligence algorithms) represents the so-called inverse problem, consisting in finding the architecture of a LCE-based metamaterial (whose design space consists of the LCE blocks geometry and spatial arrangement, mesogens orientation and transition temperature) according to the desired morphing functionality.

Declaration of Competing Interest

The authors declare that they have no known competing financial interests or personal relationships that could have appeared to influence the work reported in this paper.

Acknowledgments

The authors would like to thank the support from European Union's Horizon 2020 research and innovation programme (H2020-WIDESPREAD-2018, SIRAMM) under grant agreement No 857124.

References

[1] D. Roy, J.N. Cambre, B.S. Sumerlin, Future perspectives and recent advances in stimuli-responsive materials, Prog. Polym. Sci. 35 (2010) 278–301, https://doi.org/10.1016/j.progpolymsci.2009.10.008.
[2] R. Brighenti, Y. Li, F.J. Vernerey, Smart polymers for advanced applications: a mechanical perspective review, Front. Mater. 7 (2020) 196, https://doi.org/10.3389/fmats.2020.00196.
[3] R. Brighenti, M.P. Cosma, L. Marsavina, A. Spagnoli, M. Terzano, Laser-based additively manufactured polymers: a review on processes and mechanical models, J. Mater. Sci. (2020), https://doi.org/10.1007/s10853-020-05254-6.
[4] S. Mintchev, D. Floreano, Adaptive morphology: a design principle for multimodal and multifunctional robots, IEEE Robot. Automat. Mag. 23 (2016) 42–54, https://doi.org/10.1109/MRA.2016.2580593.
[5] R. Pfeifer, M. Lungarella, F. Iida, Self-organization, embodiment, and biologically inspired robotics, Science 318 (2007) 1088–1093, https://doi.org/10.1126/science.1145803.
[6] E.T. Roche, R. Wohlfarth, J.T.B. Overvelde, N.V. Vasilyev, F.A. Pigula, D. J. Mooney, K. Bertoldi, C.J. Walsh, A bioinspired soft actuated material, Adv. Mater. 26 (2014) 1200–1206, https://doi.org/10.1002/adma.201304018.
[7] M. Chen, J. Liu, R.E. Skelton, Design and control of tensegrity morphing airfoils, Mech. Res. Commun. 103 (2020), 103480, https://doi.org/10.1016/j.mechrescom.2020.103480.
[8] M. Pezzulla, S.A. Shillig, P. Nardinocchi, D.P. Holmes, Morphing of geometric composites via residual swelling, Soft Matter 11 (2015) 5812–5820, https://doi.org/10.1039/C5SM00863H.
[9] A.A. Bauhofer, S. Krödel, J. Rys, O.R. Bilal, A. Constantinescu, C. Daraio, Harnessing photochemical shrinkage in direct laser writing for shape morphing of polymer sheets, Adv. Mater. 29 (2017), 1703024, https://doi.org/10.1002/adma.201703024.
[10] Y. Zhu, M. Birla, K.R. Oldham, E.T. Filipov, Elastically and plastically foldable electrothermal micro-origami for controllable and rapid shape morphing, Adv. Funct. Mater. 30 (2020), 2003741, https://doi.org/10.1002/adfm.202003741.
[11] L. Jin, A.E. Forte, B. Deng, A. Rafsanjani, K. Bertoldi, Kirigami-inspired inflatables with programmable shapes, Adv. Mater. 32 (2020), 2001863, https://doi.org/10.1002/adma.202001863.
[12] P.-G. de Gennes, Physique moléculaire - réflexions sur un type de polymères nématiques, Comptes Rendus de l'Académie des Sciences B 281 (1975) 101–103.
[13] P.-G. De Gennes, J. Prost, The Physics of Liquid Crystals, Oxford University Press, 1993.
[14] P. Bladon, E.M. Terentjev, M. Warner, Transitions and instabilities in liquid crystal elastomers, Phys. Rev. E 47 (1993) R3838–R3840, https://doi.org/10.1103/PhysRevE.47.R3838.
[15] M. Warner, E.M. Terentjev, Liquid crystal elastomers, Oxford University Press, 2007.
[16] J. Kupfer, H. Finkelmann, Nematic liquid single crystal elastomers, Macromol. Chem. Rapid Commun. 12 (1991) 717–726, https://doi.org/10.1002/marc.1991.030121211.
[17] A. De Simone, L. Teresi, Elastic energies for nematic elastomers, Eur. Phys. J. E 29 (2009) 191–204, https://doi.org/10.1140/epje/i2009-10467-9.
[18] Y. Zhang, C. Xuan, Y. Jiang, Y. Huo, Continuum mechanical modeling of liquid crystal elastomers as dissipative ordered solids, J. Mech. Phys. Solids 126 (2019) 285–303, https://doi.org/10.1016/j.jmps.2019.02.018.
[19] T. White, D. Broer, Programmable and adaptive mechanics with liquid crystal polymer networks and elastomers, Nat. Mater. 14 (2015) 1087–1098, https://doi.org/10.1038/nmat4433.
[20] C.P. Ambulo, J.J. Burroughs, J.M. Boothby, H. Kim, M.R. Shankar, T.H. Ware, Four-dimensional printing of liquid crystal elastomers, ACS Appl. Mater. Interfaces 9 (42) (2017) 37332–37339, https://doi.org/10.1021/acsami.7b11851.
[21] M. Barnes, S.M. Sajadi, S. Parekh, M.M. Rahman, P.M. Ajayan, R. Verduzco, Reactive 3D printing of shape-programmable liquid crystal elastomer actuators, ACS Appl. Mater. Interfaces 12 (25) (2020) 28692–28699, https://doi.org/10.1021/acsami.0c07331.
[22] M. Barnes, R. Verduzco, Direct shape programming of liquid crystal elastomers, Soft Matter. 15 (2019) 870–879, https://doi.org/10.1039/C8SM02174K.
[23] S.K. Ahn, T.H. Ware, K.M. Lee, V.P. Tondiglia, T.J. White, Photoinduced topographical feature development in blueprinted azobenzene-functionalized liquid crystalline elastomers, Adv. Funct. Mater. 26 (32) (2016) 5819–5826, https://doi.org/10.1002/adfm.201601090.
[24] T. Ikeda, M. Nakano, Y. Yu, O. Tsutsumi, A. Kanazawa, Anisotropic bending and unbending behavior of azobenzene liquid-crystalline gels by light exposure, Adv. Mater. 15 (3) (2003) 201–205, https://doi.org/10.1002/adma.200390045.
[25] C. Huang, J. Lv, X. Tian, Y. Wang, Y. Yu, J. Liu, Miniaturized swimming soft robot with complex movement actuated and controlled by remote light signals, Sci. Rep. 5 (2015) 17414, https://doi.org/10.1038/srep17414.

[26] A. Kotikian, C. McMahan, E.C. Davidson, J.M. Muhammad, R.D. Weeks, C. Daraio, J.A. Lewis, Untethered soft robotic matter with passive control of shape morphing and propulsion, Sci. Robot. 4 (2019), https://doi.org/10.1126/scirobotics.aax7044.
[27] J. Xu, S. Chen, W. Yang, B. Qin, X. Wang, Y. Wang, Y. Dong, Photo actuation of liquid crystalline elastomer nanocomposites incorporated with gold nanoparticles based on surface plasmon resonance, Soft Matter. 15 (30) (2019) 6116–6126, https://doi.org/10.1039/C9SM00984A.
[28] H. Kim, J.A. Lee, C.P. Ambulo, H.B. Lee, S.H. Kim, V.V. Naik, T.H. Ware, Intelligently actuating liquid crystal elastomer carbon nanotube composites, Adv. Funct. Mater. 29 (48) (2019), 1905063, https://doi.org/10.1002/adfm.201905063.
[29] Y. Yang, W. Zhan, R. Peng, C. He, X. Pang, D. Shi, Z. Lin, Graphene-enabled superior and tunable photomechanical actuation in liquid crystalline elastomer nanocomposites, Adv. Mater. 27 (41) (2015) 6376–6381, https://doi.org/10.1002/adma.201503680.
[30] H.K. Bisoyi, A.M. Urbas, Q. Li, Soft materials driven by photothermal fect and their applications, Adv. Opt. Mater. 6 (2018), 1800458, https://doi.org/10.1002/adom.201800458.
[31] Q. Zhang, D. Zhang, Y. Dobah, F. Scarpa, F. Fraternali, R.E. Skelton, Tensegrity cell mechanical metamaterial with metal rubber, Appl. Phys. Lett. 113 (2018), 031906, https://doi.org/10.1063/1.5040850.
[32] M. Kadic, G.W. Milton, M. van Hecke, M. Wegener, 3D metamaterials, Nat. Rev. Phys. 1 (2019) 198–210, https://doi.org/10.1038/s42254-018-0018-y.
[33] C. Mostajeran, Curvature generation in nematic surfaces, Phys. Rev. E 91 (6) (2015), 062405, https://doi.org/10.1103/PhysRevE.91.062405.
[34] F. Feng, J.S. Biggins, M. Warner, Evolving, complex topography from combining centers of Gaussian curvature, Phys. Rev. E 102 (1) (2020), 013003, https://doi.org/10.1103/PhysRevE.102.013003.
[35] J.A. Lewis, R.G. Nuzzo, L. Mahadevan, A.S. Gladman, E.A. Matsumoto, Biomimetic 4D printing, Nat. Mater. 15 (2016) 413–418, https://doi.org/10.1038/nmat4544.
[36] A.S. Kuenstler, Y. Chen, P. Bui, H. Kim, A. DeSimone, L. Jin, R.C. Hayward, Blueprinting photothermal shape-morphing of liquid crystal elastomers, Adv. Mater. 32 (17) (2020), 2000609, https://doi.org/10.1002/adma.202000609.
[37] M. Doi, Introduction to Polymer Physics, Oxford University Press, 1996.
[38] F.J. Vernerey, R. Long, R. Brighenti, A statistically-based continuum theory for polymers with transient networks, J. Mech. Phys. Solids 107 (2017) 1–20, https://doi.org/10.1016/j.jmps.2017.05.016.
[39] M. Rubinstein, R.H. Colby, Polymer Physics, Oxford University Press, 2003.
[40] R. Brighenti, C.G. McMahan, M.P. Cosma, A. Kotikian, J.A. Lewis, C. Daraio, A micromechanical-based model of stimulus responsive liquid crystal elastomers, J. Sol. Struct. 219 (2021) 92–105, https://doi.org/10.1016/j.ijsolstr.2021.02.023.
[41] R. Brighenti, M.P. Cosma, Swelling mechanism in smart polymers responsive to mechano-chemical stimuli, J. Mech. Phys. Solids 143 (2020), 104011, https://doi.org/10.1016/j.jmps.2020.104011.
[42] S.M. Clarke, A. Hotta, A.R. Tajbakhsh, E.M. Terentjev, Effect of crosslinker geometry on equilibrium thermal and mechanical properties of nematic elastomers, Phys. Rev. E 64 (2001), 061702, https://doi.org/10.1103/PhysRevE.64.061702.
[43] A.R. Tajbakhsh, E.M. Terentjev, Spontaneous thermal expansion of nematic elastomers, Eur. Phys. J. E 6 (2001) 181–188, https://doi.org/10.1007/s101890170020.
[44] U.G.K. Wegst, H. Bai, E. Saiz, A.P. Tomsia, R.O. Ritchie, Bioinspired structural materials, Nat. Mater. 14 (2015) 23–36, https://doi.org/10.1038/nmat4089.
[45] C. Laschi, M. Cianchetti, B. Mazzolai, L. Margheri, M. Follador, P. Dario, Soft robot arm inspired by the octopus, Null 26 (2012) 709–727, https://doi.org/10.1163/156855312x626343.
[46] D. Rus, M.T. Tolley, Design, fabrication and control of soft robots, Nature 521 (2015) 467–475, https://doi.org/10.1038/nature14543.
[47] M. Wehner, R.L. Truby, D.J. Fitzgerald, B. Mosadegh, G.M. Whitesides, J.A. Lewis, R.J. Wood, An integrated design and fabrication strategy for entirely soft, autonomous robots, Nature 536 (2016) 451–455, https://doi.org/10.1038/nature19100.
[48] K. Oliver, A. Seddon, R.S. Trask, Morphing in nature and beyond: a review of natural and synthetic shape-changing materials and mechanisms, J. Mater. Sci. 51 (2016) 10663–10689, https://doi.org/10.1007/s10853-016-0295-8.
[49] F.J. Vernerey, E. Benet, L. Blue, A.K. Fajrial, S.L. Sridhar, J.S. Lum, G. Shakya, K. H. Song, A.N. Thomas, M.A. Borden, Biological active matter aggregates: Inspiration for smart colloidal materials, Adv. Colloid Interface Sci. 263 (2019) 38–51, https://doi.org/10.1016/j.cis.2018.11.006.
[50] O. Peleg, J.M. Peters, M.K. Salcedo, L. Mahadevan, Collective mechanical adaptation of honeybee swarms, Nat. Phys. 14 (2018) 1193–1198, https://doi.org/10.1038/s41567-018-0262-1.
[51] R. Wagner, T. Shen, F. Vernerey, K. Such, E. Hobbs, Construction of non-equilibrium structures by insect aggregations: the case of fire ants, Bull. Am. Phys. Soc. 65 (2020).
[52] V.S. Deshpande, R.M. McMeeking, A.G. Evans, A bio-chemo-mechanical model for cell contractility, Proc. Natl. Acad. Sci. 103 (2006) 14015–14020, https://doi.org/10.1073/pnas.0605837103.
[53] M.J. Ford, C.P. Ambulo, T.A. Kent, E.J. Markvicka, C. Pan, J. Malen, T.H. Ware, C. Majidi, A multifunctional shape-morphing elastomer with liquid metal inclusions, Proc. Natl. Acad. Sci. 116 (2019) 21438–21444, https://doi.org/10.1073/pnas.1911021116.
[54] A. Kotikian, R.L. Truby, J.W. Boley, T.J. White, J.A. Lewis, 3D Printing of liquid crystal elastomeric actuators with spatially programed nematic order, Adv. Mater. 30 (2018), 1706164, https://doi.org/10.1002/adma.201706164.
[55] Z. Wang, Z. Wang, Y. Zheng, Q. He, Y. Wang, S. Cai, Three-dimensional printing of functionally graded liquid crystal elastomer, Sci. Adv. 6 (39) (2020) eabc0034, https://doi.org/10.1126/sciadv.abc0034.
[56] M. Wang, X.-B. Hu, B. Zuo, S. Huang, X.-M. Chen, H. Yang, Liquid crystal elastomer actuator with serpentine locomotion, Chem. Commun. 56 (2020) 7597–7600, https://doi.org/10.1039/D0CC02823A.
[57] A.R. Tajbakhsh, E.M. Terentjev, Spontaneous thermal expansion of nematic elastomers, Eur. Phys. J. E 6 (2) (2001) 181–188, https://doi.org/10.1007/s101890170020.